JOURNAL OF COMPUTATIONAL PHYSICS 13, 551–568 (1973)

Self-Consistent Space-Charge-Flow Using Integral Equation Field Methods

G. L. KUSIC

Department of Electrical Engineering, University of Pittsburgh, Pittsburgh, Pennsylvania 15213

Received May 11, 1972

Integral equations are used to calculate ion beams in a self-consistent space-charge-flow simulation. A charge-free solution is found, then an iterative process is used to determine new fields and the distribution of charge within the domain.

Child's law is assumed to describe ion emission in the region of the emitter, and the remaining distribution is found by correlating trajectories representative of ions within the beam.

Integral equations lead to a straightforward formulation for the charge density immediately in front of the ion-emitter in terms of the potentials for these locations which were obtained in the previous iteration. Advantages of the integral equation approach are that field equations need be solved one time only and subsequent iterated values of the field for updated charge estimates are found by a matrix multiplication. In addition, the gradient values needed to calculate the trajectories are in analytical form. An example of a planar election flow gun is used to demonstrate the approach of this paper.

1. INTRODUCTION

In recent years electron or ion flow problems have been formulated and solved for a great number of physical configurations using digital computers to carry out the computational burden. Two fine examples of these efforts are by Boers [1] and Hamza [2]. Other examples may be found in the survey article by Amboss [3]. The simulations are often a small cost compared to the actual device construction, plus the simulation is often easier to use in a study of design variations.

The density of the ion beams may be very low, such that space-change effects are negligible as in electron optical devices [4–6] or the charge may be significant [1, 2] in which case Poisson's equation determines the fields within the device. When the space charge is a large contribution, one may employ the iterative procedure of Hamza [2] in which the fields are calculated by finite differences then the space charge is found by solving the Lorentz force laws on electrons representative of segments of the ion beam. The new estimate of the beam is used in Hamza's method to improve the field calculation until there is no further change

with successive iterations. Convergence of this method is proven for the one-dimensional case [2], and there is apparently no difficulty for two-dimensional configurations. During the process of solving for the ion motion, one is required to approximate the gradients from discrete potential values which result from the finite difference solution to Poisson's equation. Errors introduced in the resulting ion trajectories, even though small, are difficult to estimate quantitatively.

The development of integral equation methods [5–8] has provided a means for improving the space-charge flow technique of Hamza. Integral equation methods offer the advantages of less computational effort for simulations employing a large number of finite difference mesh points as well as an analytical expression for the gradients. It is the purpose of this paper to develop a space-charge flow simulation using an integral equation technique. The development will not be the most general, but the principles discussed may be readily extended to other situations.

2. The Integral Equation Approach

Consider the closed domain in $x - y$ space whose boundary consists of a combination of conductors at given potentials or else boundaries in which the potential gradient is known. In other words, the Dirichlet or Neumann boundary conditions are given. Assume also that the device has an electron-emitting cathode and the fields are such that a beam is formed. The general area of the beam is considered to be known, and perhaps may constitute the entire domain. The fields inside the domain are given by Poisson's equation

$$\nabla^2\phi(x, y) = -\rho(x, y)/\epsilon_0 , \tag{1}$$

where ϕ is the potential (volts), ρ is the space charge (C/m^3), ϵ_0 the dielectric constant of free space, and ∇ the del operator.

To solve (1) using the integral equation method, the charge on the boundaries is found by using a Green's function approach [7, 9], or alternately, one may assume the boundary has a dipole distribution [6]. The dipole assumption leads to simpler integrals and will be used here. In either case, the potential at any point in the domain may be written as

$$\phi(x, y) = \int \sigma(s)\, g_1(s, x, y)\, ds + \int g_2(x, y, x', y')\, \rho(x', y')\, dx'\, dy', \tag{2}$$

where g_1 and g_2 are the respective Green's functions, $\sigma(s)$ is the dipole distribution and the space charge is $\rho(x', y')$. Except for simple cases this integral cannot be evaluated, so that it is necessary to approximate the boundary by a series of straight line or curved segments [5, 6, 8] which may be evaluated in closed form

or lead to well known integral expressions. In addition, the continuous distribution $\rho(x, y)$ does not lend itself to closed form integration so it is necessary to approximate the function by a piecewise constant distribution.

Let the boundary of the device be closed and consist of N straight line conductor segments of finite length l_i each held at potential v_i, $i = 1, 2, \ldots, N$ and assume that each segment has a dipole charge layer. In the notation of Fig. 1, the potential

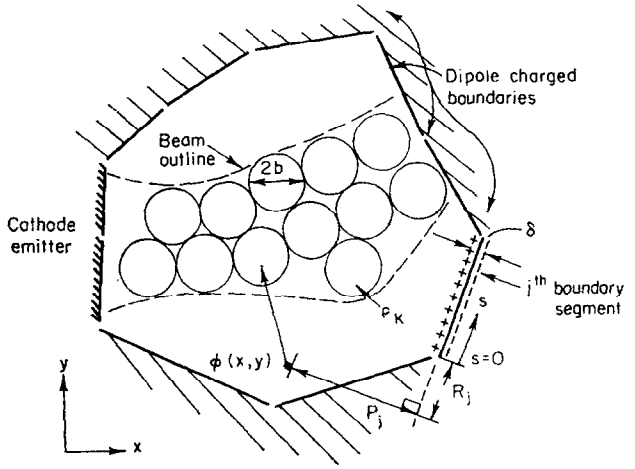

FIG. 1. Configuration of the two-dimensional charged particle beam.

at a point in the domain due to a dipole charged strip (extending infinitely in and out of the figure plane) is given by

$$\phi_j = \int_{s=0}^{l_j} \frac{\delta\sigma_j}{2\pi\epsilon_0} \left\{ \frac{P}{P^2 + (R+s)^2} \right\} ds, \tag{3}$$

where the kernal of the integral is the g_1 Green's function given in Eq. (2). Evaluating (3) the potential at (x, y) due only to segment j is

$$\phi_j(x, y) = \frac{\delta\sigma_j}{2\pi\epsilon_0} \left\{ \tan^{-1}\left(\frac{y_{j+1} - y}{x_{j+1} - x} \right) - \tan^{-1} \frac{y_j - y}{x_j - x} \right\} = \frac{\delta\sigma_j}{2\pi\epsilon_0} \theta_j, \tag{4}$$

where infinity has zero potential. For N boundary segments

$$\phi(x, y) = \frac{\delta}{2\pi\epsilon_0} \sum_{j=1}^{N} \sigma_j\theta_j + \int g_2(x, y, x', y')\, \rho(x', y')\, dx'\, dy', \tag{5}$$

and the θ_j are given by Eq. (4). Note that $\theta_1 + \theta_2 + \cdots + \theta_N = 2\pi$.

Next, in order that the potential function be bounded for all points within the space-charge region, let the space charge be approximated by M cylinders with radius b and a uniform distribution whose radii do not overlap and whose potential is given by

$$\phi_K(r) = \begin{cases} v_{0K} - \dfrac{\rho_K r^2}{4\epsilon_0} & \text{if we have} \quad r \leqslant b, \\ v_{0K} - \dfrac{\rho_K b^2}{2\epsilon_0}(\tfrac{1}{2} + \log r/b) & \text{if} \quad r \geqslant b. \end{cases} \tag{6}$$

v_{0K} is the potential at the center of the Kth cylinder of charge with reference to the dipoles. This distribution is equivalent to the assumption required when a finite difference method is directly applied to Eq. (1), in which case the potential at any meshpoint must have a density for the right side of (1) which is distributed over a mesh box surrounding this point. A point charge leads to an unbounded Green's function in subsequent steps.

Including Eq. (6) into Eq. (5) one obtains

$$\phi(x, y) = \delta/2\pi\epsilon_0 \sum_{j=1}^{N} \sigma_j\theta_j + \sum_{K=1}^{M} \{v_{0K} - (\rho_K b^2/2\epsilon_0)(\tfrac{1}{2} + \log r_K/b)\}, \tag{7}$$

where $r_K^2 = (x_k - x)^2 + (y_K - y)^2$ and (x, y) is assumed to be outside of the cylinder of charge. In order to apply the Green's function technique, Eq. (7) is evaluated for a test point at the midpoint of each of the N boundary segments whose potential is specified. This results in the matrix equation

$$\mathbf{V} = \begin{bmatrix} v_1 \\ v_2 \\ \vdots \\ v_N \end{bmatrix} = C\sigma + V_0[1]_N + E\rho, \tag{8}$$

where V_0 is a scalar sum of the reference potentials, $[1]_N$ is a column of N ones, and C is an $N \times N$ matrix with $\delta/2\epsilon_0$ on the diagonal and the sum of all elements in each row totals δ/ϵ_0. E is an $N \times M$ matrix whose elements are

$$e_{ij} = (-b^2/4\epsilon_0)[1 + \log\{(x_j - x_i)^2 + (y_j - y_i)^2\}/b^2] \tag{9}$$

and i corresponds to the midpoint of the ith boundary segment and j the coordinates of the jth charge cylinder. σ and ρ aer the vectors corresponding to the dipoles and charge in Eq. (7). For a convex domain C is both positive and diagonally dominant, so is nonsingular [9], and for a nonconvex region, it may be partitioned into nonsingular diagonal submatrices. Hence, Eq. (8) may be solved for the dipole densities on the boundary

$$\sigma = C^{-1}\{\mathbf{V} - V_0[1]_N - E\rho\}. \tag{10}$$

However, as we consider the space charge to be known, the potential at the center of each space charge cylinder must be determined by the domain and boundary potentials, so that application of Eq. (7) at these points yields

$$\Phi = F\sigma + V_0[1]_M + H\rho, \tag{11}$$

where F is an $M \times N$ matrix whose row's sum is δ/ϵ_0, $[1]_M$ is an M column of ones, and H is $M \times M$ with *zeros* on the diagonal and other elements of a form derived from Eq. (9). Organizing the derivation of Eqs. (8) and (11) in this manner leads to an expression for Φ which is significant in the space-charge-flow analysis. Next substitute Eq. (10) into Eq. (11) in order to obtain

$$\Phi = \{H - FC^{-1}E\}\rho + FC^{-1}\mathbf{V} + V_0\{[1]_M - FC^{-1}[1]_N\}. \tag{12}$$

A careful examination of the properties of the above expression shows that $FC^{-1}[1]_N = [1]_M$ at least for this case of Dirichlet boundary conditions, and, hence, the equation reduces to

$$\Phi = \{H - FC^{-1}E\}\rho + FC^{-1}\mathbf{V}. \tag{13}$$

This is a very concise expression for the potential at each of the charge cylinder centers. If one reflects Neumann type boundaries about the line on which they are given, it can be argued that an expression such as (13) is also obtained, but of correspondingly higher order. Equation (13) demonstrates the linearity of the analysis to this point in the sense that the field potential is the superposition of space charge and applied boundary potentials. Furthermore, there is no restriction on the number of cylinders which approximate the ion or electron beam as one may select $M \geqslant N$ or $M < N$.

3. Space-Charge-Flow Calculation

The self-consistent space-charge-flow simulation [2] is shown schematically in Fig. 2. The process is started by the input of the device geometry, physical materials and initial space charge density $\rho(x, y) = 0$ (although an initial guess may be made for ρ). The active emitter surface shown in Fig. 1 has charged particles drawn from it or suppressed according to the local normal fields. Specifically, the emitter is considered a planar diode which emits according to Child's law

$$J_d = (4/9)\,\epsilon_0(2q/m)^{1/2}(1/d)^2(\phi_d - \phi_e)^{3/2}, \tag{14}$$

where the following definitions are used: $J_d \equiv$ current density (A/m^2); $\epsilon_0 \equiv 8.855 \times 10^{-12}$ F/m; $q/m \equiv$ ratio of ion charge to rest mass (C/Kg);

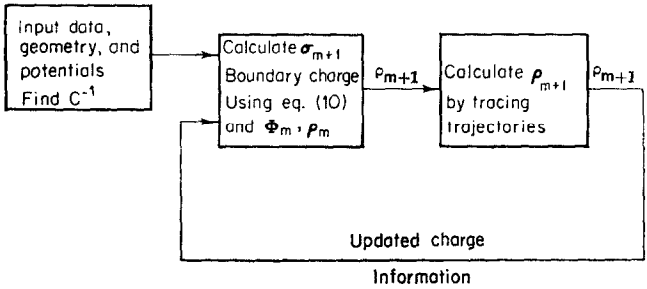

FIG. 2. General flow chart for space-charge-flow simulation.

$\phi_e \equiv$ emitter voltage; $\phi_d \equiv$ field voltage at distance d away from emitter; $d \equiv$ distance in meters from emitter to point ϕ_d.

It is clear that Eq. (14) must have $\phi_d - \phi_e > 0$ in order that negative ions be drawn from the emitter, which implies that d is outside a possible space-charge cloud in the vicinity of the emitter. If $\phi_d - \phi_e \leqslant 0$ this region of the emitter is "cut off" and it is seen that estimates of the active area could change with iteration in Fig. 2. This may be especially true for high current density devices.

Given that the active area of the emitter is closely estimated, then within the beam at every point

$$J = \rho\gamma, \tag{15}$$

where γ is the beam velocity (m/sec). Equation (14) represents the initial or starting set of values for Eq. (15) with the velocity given by $\gamma_d^2 = 2(\phi_d - \phi_e)q/m$. In order to obtain subsequent values for ρ and γ, it is necessary to trace the trajectories of selected ions through the device [1, 2]. These are considered representative of ions emitted in the immediate area and their location is determined from electric and magnetic forces on the ion given by the Lorentz force law

$$d\bar{V}/dt = q/m(\bar{E} + \bar{V} \times \bar{B}), \tag{16}$$

where the symbols have their usual meanings in $x - y$ coordinates. The magnetic fields may be due to permanent magnet pole pieces, excited coils external to the device, or from the self-generated field of the current beam. It is assumed in this analysis that the magnetic field effects are small. Notice that using Φ found from Eq. (13) and σ then given by Eq. (10), that Eq. (7) may be analytically differentiated to yield the exact gradient at any point, e.g.,

$$-E_y = \frac{\partial\phi}{\partial y}(x, y) = \frac{\delta}{2\pi\epsilon_0}\sum_{j=1}^{N}\sigma_j\frac{\partial\theta_j}{\partial y} + \sum_{K=1}^{M}\frac{\rho_K b^2}{2\epsilon_0}\left\{\frac{1}{r_K}\right\}\frac{\partial r_K}{\partial y}, \tag{17}$$

where one term of the summation $K = 1,..., M$ uses the alternate form of Eq. (6) if (x, y) lies inside a charge cylinder. The accuracy of calculating trajectories by Eq. (16) is dependent on the field data and numerical integration routine. One thereby avoids the problem of approximating the gradient from discrete potential data when using integral equations.

The trajectories are assumed to start at the cathode with zero tangential velocity, This is done for simplicity, and effects such as chromatic aberrations which define crossover beams widths and ultimately screen spot sizes should be treated by considering a distribution in ion normal and tangential emission energies [3, 5]. Usually the principal ray ion normal energy used in Child's law is a very small percentage of the total energy the ion acquires in the simulation. In selecting the number and location of trajectories at the cathode, one employs some "rule of the thumb" such as developed in Ref. [1] which found that at least one trajectory per finite difference mesh at the cathode should be used to prevent convergence to an incorrect answer. In the integral equation one may reach the same conclusion, for the analogous situation is the boundary should be finely subdivided in the cathode area because this is the most critical region of the device.

The current density profile found at the cathode by Child's law, Eq. (14), is fitted with a $p - 1$ order normalized polynomial

$$J_0(y) = \sum_{K=0}^{p-1} a_K y^K \qquad 0 \leqslant y \leqslant 1, \tag{18}$$

where p represents the number of trajectories traced through the device. At locations "downstream" where charge density data is required for subsequent iterations, a correlation is set up to compare the new distribution with cathode. (A line of reference, or beam symmetry line is very useful in the correlation.) This yields a scatter of points in the first quadrant of a planar graph. If the x-axis is a line of symmetry, a second polynomial is used in a "least-squares" fit through, the set of points (for notation purposes, $Z = y$)

$$\text{corr} = \sum_{l=1}^{L} c_l Z^l, \tag{19}$$

and the best c_l coefficients minimize the quadratic performance index

$$\text{error} = \sum_{K=1}^{p-1} \left\{ y_{K0} - \sum_{l=1}^{L} c_l Z_{Kl}^l \right\}^2. \tag{20}$$

In this last expression y_{K0} represents the cathode (initial) y location of the trajectory

and Z_{Ki} represents its y location at some downstream location. Using these values of c_l, the new current distribution is

$$J_i(y) = \left\{\sum_{K=0}^{p-1} a_K y^K\right\}\left\{\sum_{l=1}^{L} l c_l y^{l-1}\right\} \alpha, \tag{21}$$

where α is a normalization factor used to assure continuity at the new location

$$1.0 = \frac{\text{(emitter current)}}{\int_y J_i(y)\, dy}. \tag{22}$$

Notice that beam dispersions are possible in the derivation of Eqs. (19)–(22). As the final step, the charge density is obtained by

$$\rho_{ij} = J_i(y_j)/v_{\text{av.}}, \qquad \text{where} \quad v_{\text{av.}} = 1/p \sum_{K=1}^{p} v_{Ki}, \tag{23}$$

where $v_{\text{av.}}$ is the average velocity over all trajectories at the ith location.

There are other and perhaps more suitable methods to calculate the charge density throughout the device. However, in any of these methods, the fundamental assumption is that cathode emission is space charge limited by the field immediately in front of the cathode and described by Child's law. Subsequent calculations for the downstream beam current density and velocity are deterministic, bounded functions of the initial beam conditions given by Child's law and modified by Eq. (16). Therefore, in order to establish the iterative scheme shown in Fig. 2 does converge for the self-consistent calculation, it is sufficient to prove that the charge density in front of the emitter is a stable calculation versus iteration. This property may be derived from Eq. (13).

4. Convergence Considerations

In Eq. (13), let the Φ vector be partitioned such that the first p elements represent the potentials at normal distance, b, from the cathode. Trajectories are to be calculated through these points. At these locations the charge density for the $(m + 1)$ iteration is calculated from the field of the mth iteration as given by Child's law

$$\rho_i\,|_{m+1} = (4\epsilon_0/9b^2)(\phi_i - \phi_e)|_{m\text{th iteration}} \qquad i = 1, 2, \ldots, p, \tag{24}$$

and one may choose $\phi_e = 0$ with no loss in generality. Then an iterative scheme to calculate new values for the space charge in front of the cathode as shown in Fig. 2 is

$$\rho_i\,|_{m+1} = \rho_i\,|_m + \omega[\text{error}] = \rho_i\,|_m + \omega[(4\epsilon_0/9b^2)\,\phi_i\,|_m - \rho_i\,|_m], \tag{25}$$

where ω is called the relaxation factor. In terms of the ρ vector the above equation is

$$\rho\,|_{m+1} = (1 - \omega)\, I\rho\,|_m + (\omega 4\epsilon_0/9b^2)\{H - FC^{-1}E\}\rho\,|_m + (\omega 4\epsilon_0/9b^2)\, FC^{-1}\mathbf{V}, \quad (26)$$

where the $i = 1, 2, 3, \ldots, p$ elements are of concern here. This iterative scheme converges to a steady solution [9] if the eigenvalues of the $M \times M$ matrix

$$G = (1 - \omega)I + (\omega 4\epsilon_0/9b^2)\{H - FC^{-1}E\} \quad (27)$$

are less than unity in absolute magnitude. A meaningful bound in the eigenvalues is difficult to obtain from the G matrix, but a numerical example will demonstrate convergence and a dependency on the parameter ω.

It is noteworthy that integral equations in a self-consistent field calculation require the inverse C^{-1} to be calculated only one time. In Eq. (13) $FC^{-1}\mathbf{V}$ is a constant vector and $H - FC^{-1}E$ is a constant matrix used to repeatedly calculate new values of Φ.

5. An Example

Consider the electron gun design discussed by Pierce [10] which is shown in Fig. 3. This is one of the few closed form solutions [11] available to check the theory of the preceding sections. The electron flow in the x-direction is assumed to

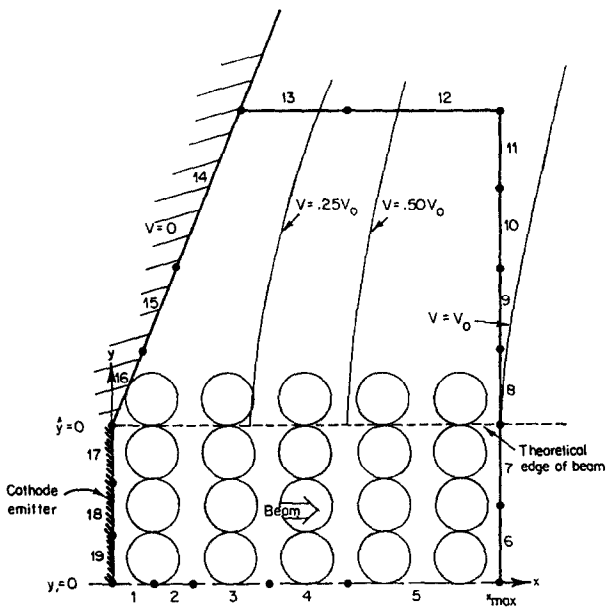

FIG. 3. The rectilinear electron flow gun of Pierce and the integral equation.

be space-charge-limited, and to be emitted from a cathode forming the boundary $x = 0$. The current density in the beam is given by Eq. (14) and the closed form solution [10] for potentials in the region outside the beam is

$$\phi = \frac{V_0}{(X_{\max})4/3} \text{Real}\{(x + j\hat{y})^{4/3}\} \qquad V_0 = 10{,}000, \quad X_{\max} = 0.05, \tag{28}$$

where V_0 is the maximum voltage applied at $x = x_{\max}$ and $j = \sqrt{-1}$. The above equation indicates the plane at $\theta = 67.5° = \tan^{-1}(\hat{y}/x)$, along with the cathode, is at zero potential.

In order to provide a meaningful test for the integral equation method presented in this paper, a boundary is taken of 19 irregular length segments as indicated in Fig. 3. The plane $y = 0.0$ is assumed to be one of symmetry and, hence, has Neumann boundary conditions. The boundary segments, their coordinates and boundary conditions are tabulated in Table I. The spacing of the dipoles (Eq. (3)), is $\delta = 0.000825$. With this starting point, the beam and potentials are to be calculated and compared with Eqs. (14) and (28).

We initially assume the beam consists of 20 charge cylinders of radius $b = 0.00333$ and distributed at coordinates $(x_i, y_K) = (0.005 + 0.01i, b + 2bK)$ for $i = 0, 1, 2, 3, 4$ and $K = 0, 1, 2, 3$. As the program progresses through its iterations charge densities will be assigned to the cylinders, but some may be zero as determined by the "edge" of the beam. Notice that voids appear between the cylinders. If we multiply the calculated charge by $6/\pi$ this increases the effective charge by the ratio of the rectangle area to circle area and thereby accounts for the void areas.

For this problem we compute four trajectories, (although more could be used) from $x = 0.005$ to $x = 0.045$ using the gradients calculated by forms similar to Eq. (17). A two-step Runge–Kutta process was used to integrate these nonlinear equations of motion, $dZ/dt = f(Z)$, as follows:

$$Z(n\tau + \tau) = Z(n\tau) + a_1\tau P + a_2\tau Q, \tag{29}$$

where the quantities are defined below

$$P = f(Z(n\tau)) = \begin{bmatrix} \dfrac{dx}{dt}(n\tau) \\ \dfrac{-q}{m}\dfrac{\partial\phi}{\partial x}(n\tau) \\ \dfrac{dy}{dt}(n\tau) \\ \dfrac{-q}{m}\dfrac{\partial\phi}{\partial y}(n\tau) \end{bmatrix} \qquad \begin{aligned} Q &= f(Z(n\tau + a_3\tau), n\tau + a_3\tau) \\ a_1 &= a_2 = \tfrac{1}{2} \\ a_3 &= 1 \end{aligned}$$

TABLE I

Boundary Data for Example of Section 5

x, y coordinates	segment	Boundary condition
0, 0		
	1	$\partial\phi/\partial y = 0$
0.005, 0		
	2	$\partial\phi/\partial y = 0$
0.01, 0		
	3	$\partial\phi/\partial y = 0$
0.02, 0		
	4	$\partial\phi/\partial y = 0$
0.03, 0		
	5	$\partial\phi/\partial y = 0$
0.05, 0		
	6	$\phi = 10{,}000$
0.05, 0.01		
	7	$\phi = 10{,}000$
0.05, 0.02		
	8	$\phi = 9977$
0.05, 0.03		
	9	$\phi = 9802$
0.05, 0.04		
	10	$\phi = 9456$
0.05, 0.05		
	11	$\phi = 8954$
0.05, 0.06		
	12	$\phi = 5894$
0.03, 0.06		
	13	$\phi = 1609$
0.0167, 0.06		
	14	$\phi = 0$
0.0082, 0.04		
	15	$\phi = 0$
0.0041, 0.03		
	16	$\phi = 0$
0, 0.020		
	17	$\phi = 0$
0, 0.0133		
	18	$\phi = 0$
0, 0.0067		
	19	$\phi = 0$
0, 0		

In this equation Z is a four element column vector of the trajectory state—x-position, x-velocity, y-position, and y-velocity. The time step τ was chosen such that the space displacement per call of the Runge–Kutta was approximately $\Delta x = 0.002$. For this example it was believed that increased accuracy of say a four-step Runge–Kutta, or more refined space increments was not necessary. One should notice that each call on the Runge–Kutta routine requires both x and y direction gradients to be calculated from 19 boundary segments plus 20 distributed charge cylinders, so an increase in accuracy costs more computer time. The trajectory initial conditions are extremely critical and are discussed below.

As the trajectories are calculated up to each charge plane, $x(i) \cong 0.005 + 0.01i$, $i = 0, 1, 2, 3, 4$ a new charge density is obtained for the present iteration. Child's law and the velocity calculated at $x = 0.005$ define the beam at this location. The beam is assumed to be of uniform density in the y-direction, so the charge density is taken as the average (a_0 in Eq. (18)) from the four trajectories traced. At subsequent locations $x \cong 0.015$, 0.025, 0.035, 0.045, the correlation polynomial Eq. (19), is taken to be $c_1 Z$ and c_1 then appears in Eq. (21) as a multiplier. The next step is determine the "edge" of the beam which is found by examining the y position of the trajectory which defined the edge of the beam at the cathode (or the maximum y for all trajectories). It is easily seen that the y-coordinate of this trajectory, if it does not intersect other trajectories, fixes the number of vertical direction charge cylinders at each x-station by

$$\begin{aligned} y(4) &> 0.030, && > 4 \text{ cylinders}, \\ 0.023 < y(4) &\leqslant 0.030, && 4 \text{ cylinders}, \\ 0.0167 < y(4) &\leqslant 0.023, && 3 \text{ cylinders}, \\ 0.010 < y(4) &\leqslant 0.0167, && 2 \text{ cylinders}, \\ 0 < y(4) &\leqslant 0.010, && 1 \text{ cylinders}, \end{aligned} \tag{30}$$

which is an option routine in the computer program. Finally, the average x-direction velocity is used in Eq. (23) to calculate the charge densities. The problem of the edge of the beam also arises in other trajectory-tracing methods [2].

To begin the iterative scheme of Fig. 2, $\rho = 0$ and the matrix C^{-1} is calculated using the input data of Table I. For the first iteration when the space charge is absent the trajectory data is tabulated in Table II, part A. The trajectories initial conditions are evident in the table. Using the relaxation factor $\omega = 0.5$, the computer program went through additional iterations in order to obtain the trajectory data tabulated for the fifth iteration presented in part B of Table II. In Table III, the calculated potentials and densities are compared with the true solution, where it may be seen the errors are within 6% of the true values. Considering the small number of boundary segments which were used, this is a good

TABLE II

Iteration Results for Example Problem, $\omega = 0.50$

A-first iteration, $\rho = 0$, $\tau \equiv$ time increment

	Trajectory	x-position	x-velocity	y-position	y-velocity
	1	0.004	$0.187 \times 10^{+7}$	0.005	0.0
	2	0.004	$0.187 \times 10^{+7}$	0.010	0.0
	3	0.004	$0.187 \times 10^{+7}$	0.015	0.0
	4	0.004	$0.187 \times 10^{+7}$	0.020	0.0
$\tau = 1.6 \times 10^{-10}$					
	1	0.637×10^{-2}	0.130×10^{8}	0.498×10^{-2}	0.213×10^{6}
	2	0.630×10^{-2}	0.125×10^{8}	0.991×10^{-2}	0.637×10^{6}
	3	0.618×10^{-2}	0.118×10^{8}	0.148×10^{-1}	0.128×10^{7}
	4	0.619×10^{-2}	0.118×10^{8}	0.196×10^{-1}	0.231×10^{7}
$\tau = 0.9 \times 10^{-10}$					
	1	0.162×10^{-1}	0.290×10^{8}	0.448×10^{-2}	0.203×10^{7}
	2	0.157×10^{-1}	0.282×10^{8}	0.924×10^{-2}	0.237×10^{7}
	3	0.151×10^{-1}	0.272×10^{8}	0.137×10^{-1}	0.349×10^{7}
	4	0.151×10^{-1}	0.271×10^{8}	0.178×10^{-1}	0.523×10^{7}
$\tau = 0.7 \times 10^{-10}$					
	1	0.259×10^{-1}	0.395×10^{8}	0.384×10^{-2}	0.272×10^{7}
	2	0.251×10^{-1}	0.385×10^{8}	0.840×10^{-2}	0.352×10^{7}
	3	0.270×10^{-1}	0.399×10^{8}	0.121×10^{-1}	0.529×10^{7}
	4	0.270×10^{-1}	0.398×10^{8}	0.156×10^{-1}	0.731×10^{7}
$\tau = 0.6 \times 10^{-10}$					
	1	0.364×10^{-1}	0.486×10^{8}	0.304×10^{-2}	0.501×10^{7}
	2	0.353×10^{-1}	0.472×10^{8}	0.741×10^{-2}	0.501×10^{7}
	3	0.375×10^{-1}	0.485×10^{8}	0.107×10^{-1}	0.653×10^{7}
	4	0.374×10^{-1}	0.485×10^{8}	0.137×10^{-1}	0.849×10^{7}
$\tau = 0.5 \times 10^{-10}$					
	1	0.474×10^{-1}	0.541×10^{8}	0.195×10^{-2}	0.294×10^{7}
	2	0.462×10^{-1}	0.542×10^{8}	0.626×10^{-2}	0.506×10^{7}
	3	0.458×10^{-1}	0.542×10^{8}	0.966×10^{-2}	0.659×10^{7}
	4	0.458×10^{-1}	0.545×10^{8}	0.123×10^{-1}	0.876×10^{7}
		B-fifth iteration, $\rho \neq 0$, $\tau \equiv$ time increment			
$\tau = 2 \times 10^{-10}$	1	0.674×10^{-2}	0.116×10^{8}	0.502×10^{-2}	0.158×10^{5}
	2	0.669×10^{-2}	0.112×10^{8}	0.995×10^{-2}	0.265×10^{6}
	3	0.666×10^{-2}	0.111×10^{8}	0.148×10^{-1}	0.670×10^{6}
	4	0.698×10^{-2}	0.123×10^{8}	0.199×10^{-1}	0.112×10^{6}
$\tau = 1 \times 10^{-10}$					
	1	0.175×10^{-1}	0.283×10^{8}	0.472×10^{-2}	0.935×10^{6}
	2	0.171×10^{-1}	0.278×10^{8}	0.961×10^{-2}	0.103×10^{7}
	3	0.170×10^{-1}	0.276×10^{8}	0.142×10^{-1}	0.143×10^{7}
	4	0.150×10^{-1}	0.252×10^{8}	0.200×10^{-1}	0.121×10^{5}

Table continued

TABLE II *(continued)*

	Trajectory	x-position	x-velocity	y-position	y-velocity
$\tau = 0.7 \times 10^{-10}$					
	1	0.250×10^{-1}	0.372×10^{8}	0.450×10^{-2}	0.126×10^{7}
	2	0.275×10^{-1}	0.395×10^{8}	0.921×10^{-2}	0.165×10^{7}
	3	0.272×10^{-1}	0.391×10^{8}	0.137×10^{-1}	0.199×10^{7}
	4	0.273×10^{-1}	0.391×10^{8}	0.199×10^{-1}	0.333×10^{6}
$\tau = 0.6 \times 10^{-10}$					
	1	0.355×10^{-1}	0.476×10^{8}	0.407×10^{-2}	0.307×10^{7}
	2	0.354×10^{-1}	0.468×10^{8}	0.883×10^{-2}	0.253×10^{7}
	3	0.351×10^{-1}	0.464×10^{8}	0.133×10^{-1}	0.247×10^{7}
	4	0.352×10^{-1}	0.464×10^{8}	0.198×10^{-1}	0.575×10^{6}
$\tau = 0.5 \times 10^{-10}$					
	1	0.467×10^{-1}	0.548×10^{8}	0.333×10^{-2}	0.216×10^{7}
	2	0.466×10^{-1}	0.555×10^{8}	0.823×10^{-2}	0.247×10^{7}
	3	0.463×10^{-1}	0.556×10^{8}	0.127×10^{-1}	0.258×10^{7}
	4	0.464×10^{-1}	0.558×10^{8}	0.197×10^{-1}	0.639×10^{6}

TABLE III

Beam Results After Fifth Iteration for Trajectories of Table II

		Calculated beam potentials (V)				
↑	0.0167	427	2078	4097	6324	8700
y-position	0.0100	461	2119	4173	6421	8668
	0.0033	490	2157	4250	6751	8361
x-position →		0.005	0.015	0.025	0.035	0.045
		True beam potentials (Eq. (V.1))(V)				
		465	2009	3969	6216	8690
x-position →		0.005	0.015	0.025	0.035	0.045
		Calculated beam current density (A/m^2)				
		969	965	980	960	970
x-position →		0.005	0.015	0.025	0.035	0.045

(True beam density = 942 amps/m^2)

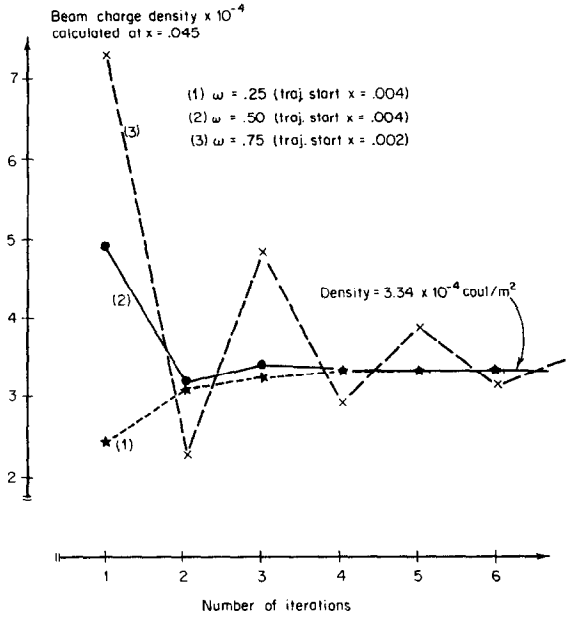

FIG. 4. Space-charge density versus iteration.

degree of accuracy. The convergence properties of the system are illustrated in Fig. 4.

Due to singularities in the gradient at the end-points of the boundary segments, the initial conditions on the trajectories are very critical. Small errors at this point tend to be magnified by the time a trajectory reaches its termination. For example, the same initial velocity 0.187×10^7 m/sec was used for trajectories starting at $y_i = 0.005i$, $x = 0.002$, 0.003, and 0.004 but the terminal results (*charge-free*) are as follows

		start at $x = 0.002$	start at $x = 0.003$	start at $x = 0.004$
terminal y-position at $x \cong 0.045$	$i = 1$	0.0030	0.0024	0.0020
	$i = 2$	0.0072	0.0066	0.0063
	$i = 3$	0.0097	0.0097	0.0097
	$i = 4$	0.0101	0.0117	0.0123

These trends were also present after the program calculated the distributed beam charge and moved the trajectories closer to the theoretical true solution (compare part A and part B of Table II). Some attempts were also made to start the trajec-

tories without x-velocity, but the results were very poor, hence, the small initial electron energy shown in Table II was important. This initial energy is a small percentage of the maximum beam energy, so it is a valid approximation. A general rule applicable to large, detailed simulations would be to use a refined boundary in the vicinity of the cathode then start the electrons from one boundary segment away from the cathode with the energy of the field at that point. This would yield good trajectory results.

In this example problem, the IBM 360 model 60 computer operating time was 70 sec to set up the example and calculate C^{-1}. An additional 20 sec was required to calculate trajectories and charge distributions for eight iterations. This is a "first-pass" programming effort and could be improved.

6. Concluding Remarks

The theories of Sections 2–4 were essentially verified with the example of Section 5. However, the example also indicated some restrictions when applying the integral equation methods to general problems. Among the first of these considerations is the number of and the length of the segments which comprise the boundary of the device. A second consideration is the number of assumed charge cylinders. If one assumes a greater number of segments and cylinders than necessary, the computer running time will be accordingly greater with some increase in accuracy. The example problem did not indicate any computer "round-off" errors using a 32-bit machine. Therefore, one could refine the boundaries and segments by orders of magnitude before machine errors began to affect the calculation. When the number of charge cylinders effectively in the beam was increased from 10 to 15, there was a significant increase in accuracy. An improvement in accuracy was gained by refining the boundary in the vicinity of $x = 0$, $y = 0.0$ from original lengths of 0.01 to those indicated in Fig. 3. This is the region of very low electron velocity and is accordingly sensitive to gradient errors. For general problems this area should be refined compared to "far out" regions, for example near segments #5 and #14.

Another consideration of the integral equation method is the singularity which exists at the end points of the boundary segment. While the dipole assumption allows one to use the Green's function at the center of a boundary segment, the fields and especially the gradients (e.g. see Eq. (17)) are not calculable at the end points. In the example of Section 5, initial conditions for the trajectories were assumed a small distance away from the cathode. When an attempt was made to "start electrons from rest" along the cathode, large errors appeared for motion tangential to the boundary segment even when the starting point was not in the vicinity of a segment endpoint.

There are several advantages in using the integral equation formulation as compared to, for instance, a finite difference approach. The principal advantage is that the C matrix of Eq. (8) uses N boundary segments, and, hence, the matrix is $N \times N$ while the equivalent finite difference system matrix is $N^2/16 \times N^2/16$. These matrices must be inverted and the inverse used repeatedly in the process of iterating to calculate the beam. Hence, larger simulations will be more efficient using integral equation methods. A second major advantage is the gradient is available in the integral equation method while it must be approximated in a finite difference scheme. Even though the contributions of all boundary and distributed charges must be included using the integral equation method, this is an efficient "DO LOOP" in a computer program and does not consume much time.

In the integral equation approach, as well as any other method to calculate an electron beam, there are many "rules of thumb" or "computing experience" such as the best number of boundary segments, number of trajectories, good starting guesses for the beam, etc. which may be used to reduce the cost of computation. Given a range of applications, these techniques will develop in the future for the integral equation approach.

ACKNOWLEDGMENTS

The author wishes to express his gratitude to Professor R. Duffin of Carnegie Mellon University and Dr. T. Vogl of Westinghouse Research who were instrumental in providing initial ideas which led to this paper. The author also wishes to thank the reviewer whose examination of the first draft led to a more accurate, concise presentation.

REFERENCES

1. J. E. BOERS, Digital computer analysis of electron flows, Proc. Electron and Laser Beam Symposium, Pennsylvania State University, University Park, April 2, 1965.
2. V. HAMZA, NASA Report, No. TND-1711, Washington, D. C., 1963.
3. K. AMBOSS, The analysis of dense electron beams, *in* "Advances in Electronics and Physics," Academic Press, New York, 1969.
4. J. VINE, Electron optical ray tracing in cathode lenses, *IEEE Trans. Electron Devices* **ED-13** (1966).
5. B. SINGER AND M. BRAUN, Integral equation methods for computer evaluation of electron optics, *IEEE Trans. Electron Devices* **ED-17** (1970).
6. G. L. KUSIC, Optimal design of electrostatic lenses using integral equation methods, *IEEE Trans. Electron. Devices* **ED-18**, No. 10 (1971).
7. R. F. HARRINGTON, "Field Computation by Moment Methods," Chapter 2, Macmillan, New York, 1968.

8. R. F. HARRINGTON, K. PONTOPPIDAN, P. ABRAHAMSEN, AND N. C. ALBERTSEN, Computation of Laplacian potentials by an equivalent source method, *British IEE Proceedings* **116** (1969).
9. R. S. VARGA, "Matrix Iterative Analysis," Prentice-Hall, New York, 1962.
10. J. R. PIERCE, "Theory and Design of Electron Beams," Van Nostrand, New York, 1949.
11. J. R. ASHLEY, Hybrid Computer Aided Design of Thick Electrostatic Electron Lenses, *Proc. IEEE* **60** (1972.